AIRS Deconvolution and Translation from the AIRS to CrIS IR Sounders

**** DRAFT ****

Howard E. Motteler
L. Larrabee Strow

UMBC Atmospheric Spectroscopy Lab
Joint Center for Earth Systems Technology

September 8, 2017

1 Introduction

Upwelling infrared radiation as measured by the AIRS [1] and CrIS [2, 6] sounders is a significant part of the long term climate record. We would like to treat this as a single data set and often want to compare radiances, for example in the analysis of simultaneous nadir overpasses (SNOs) for sounder calibration or validation. However the instruments have different spectral resolutions, channel response functions, and band spans. As a step in addressing this problem we consider the translation of channel radiances from AIRS to standard resolution CrIS.

In addition to AIRS to CrIS we make regular use of an IASI to CrIS translation, and have implemented and tested IASI to AIRS and CrIS to AIRS translations as well. The translations from IASI includes deapodization (a form of deconvolution) before reconvolution to the translation target and work very well. Ranking these translations by accuracy in comparison with calculated reference truth, we have IASI to CrIS, IASI to AIRS, AIRS to CrIS, and finally CrIS to AIRS [**?**]. But aside from the AIRS to CrIS translation, the methods used are for the most part conventional.

Our translation from AIRS to CrIS has some novel features. AIRS is a grating spectrometer with a distinct response function for each channel determined by the focal plane geometery, while CrIS is a Michaelson interferometer with a sinc response function, after calibration and corrections.

In section 2 we show how to take advantage of our detailed knowledge of the AIRS spectral response functions (SRFs) and their overlap to deconvolve channel radiances to a resolution-enhanced intermediate representation, typically a 0.1 cm^{-1} grid, the approximate resolution of the tabulated AIRS SRFs. This intermediate representation can then be reconvolved to an alternate instrument specification. Section 3 gives details and validation tests for the AIRS to CrIS translation and section 4 for translation to an idealized grating model. For both cases deconvolution followed by reconvolution is shown to work significantly better than conventional interpolation. Both methods can be further improved with a statistical correcion. In section 5 we consider a purely statistical approach to such translations. Section 6 discusses applications and related and future work.

2 AIRS Deconvolution

The AIRS spectral response functions model channel response as a function of frequency and associate channels with nominal center frequencies. Each AIRS channel i has an associated spectral response function or SRF $\sigma_i(v)$ such that the channel radiance $c_i = \int \sigma_i(v) r(v)\, dv$, where r is radiance at frequency v. The center or peak of σ_i is the nominal channel frequency.

Figure 1 shows typical AIRS SRFs from the low and high ends of the band. Note the significant overlap in the wings. This can allow for a deconvolution to recover resolution beyond that of the response functions considered individually. The SRFs are not necessarily symmetrical, especially at the high end of the band. The dashed line on top of the third SRF in each group is a fit for a generalized Gaussian, which we consider in more detail later in this section. Figure 2 shows channel spacing and resolving power for the AIRS L1c channel set [**?**]. The variable channel spacing and resolving power are due to the modular structure of the focal plane. Although not entirely regular—that is, not a simple function of frequency—the L1c channel set is more regular than the L1b channel set from which it is derived, and we mainly consider the L1c set here.

Suppose we have n channels and a frequency grid $\vec{v}$ of k points spanning the union of the domains of the functions σ_i. The grid step size for our applications is often 0.0025 cm^{-1}, the default resolution for upwelling radiances calculated with kcarta [4]. Let S_k be an $n \times k$ array such that $s_{i,j} = \sigma_i(v_j)/w_i$, where $w_i = \sum_j \sigma_i(v_j)$, that is where row i is $\sigma_i(v)$ tabulated at the grid $\vec{v}$ and normalized so the row sum is 1. If the channel centers are in increasing order S_k is banded, and if they are not too close (as is the case

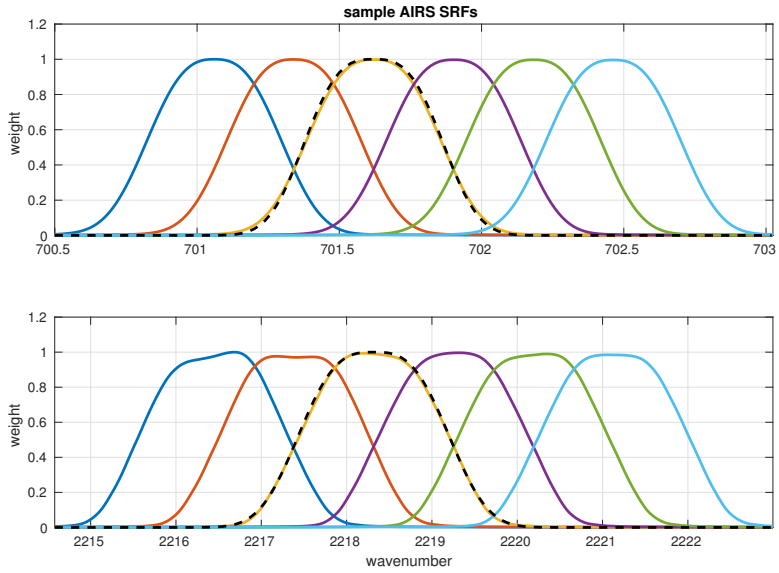

Figure 1: sample AIRS spectral response functions from the low and high ends of the band. The dashed line is a generalized Gaussian function.

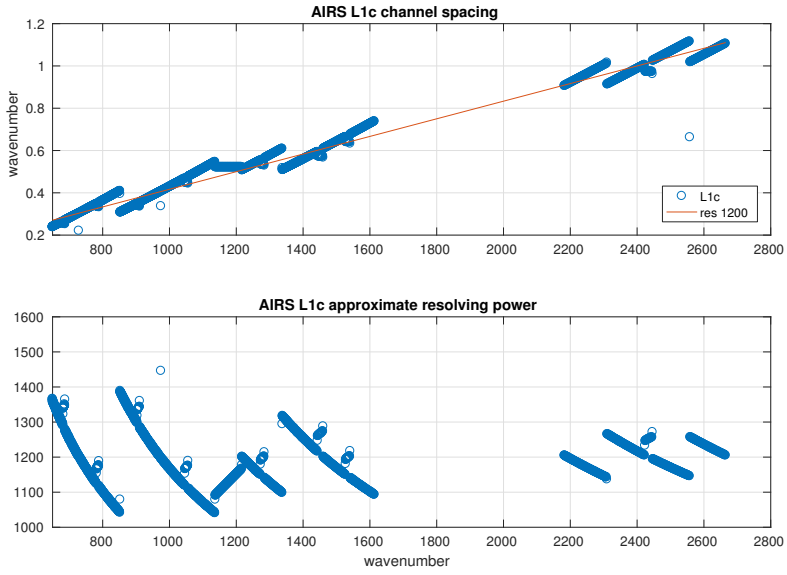

Figure 2: AIRS L1c channel spacing and derived resolving power.

for a few of the L1b channels) the rows are linearly independent. S_k is a linear transform whose domain is radiance at the grid $\vec{v}$ and whose range is channel radiances. If r is radiance at the grid $\vec{v}$, then $c = S_k r$ gives a good approximation of the channel radiances $c_i = \int \sigma_i(v) r(v)\, dv$. In practice this is how we convolve kcarta or other high resolution calculated radiances to get AIRS channel radiances, for example for reference truth or "true AIRS" for the tests shown here.

For the AIRS to CrIS and other translations we are mainly interested in the transform S_b for SRFs at an intermediate resolution, typically 0.1 cm^{-1}. This is the approximate resolution of the SRF measurements and convenient for reconvolution to the CrIS user grid. So let $\vec{v}_b = v_1, v_2, \ldots, v_m$ be a 0.1 cm^{-1} grid spanning the domains of the functions σ_i. Similar to S_k, let S_b be an $n \times m$ array where row i is $\sigma_i(v)$ tabulated at the $\vec{v}_b$ grid, with rows normalized to 1. If r is radiance at the $\vec{v}_b$ grid, then $c = S_b r$ is still a reasonable approximation of $\int \sigma_i(v) r(v)\, dv$.

For our application we want to start with c and find r, that is to deconvolve c by solving $S_b r = c$ for r. Since $m < k$ the system is underdetermined. We take the Moore-Penrose pseudoinverse [**?**] of S_b to get $r_0 = S_b^{-1} c$. This gives a minimal solution, in the sense that $||r_0||_2 \leq ||r_j||_2$ for all r_j satisfying $S_b r_j = c$. The condition number for S_b as built from the L1c channels is $||S_b||_2 ||S_b^{-1}||_2 = 115$, which is tolerable.

Although our main goal is to reconvolve the 0.1 cm^{-1} intermediate representation to the CrIS or other user grids, we first compare the deconvolved radiances with reference truth from a direct convolution to the intermediate grid. The choice of response functions for the direct convolution is not obvious, since the deconvolution is undoing—at least to some extent—the effects of the AIRS SRF convolutions. We chose a generalized Gaussian of the form

$$w(v, v_0, \text{FWHM}) = \exp\left(-\left(\frac{(v - v_0)^2}{2c^2}\right)^{1.5}\right)$$

where $c = \text{FWHM}/(2\sqrt{2 \ln 2})$ and v_0 is the desired channel center. The exponent 1.5 was chosen to give an approximate match to AIRS SRFs with the same FWHM and channel centers, though without the fine structure and variation of the measured SRFs. Figure 1 shows two such generalized Gaussians paired with the corresponding AIRS SRFs. We used the same functions as reference truth for the 0.1 cm^{-1} intermediate grid with $\text{FWHM} = v_i/2000$, where v_i are the grid frequencies. This represents a hypothetical grating spectrometer with a resolving power of 2000, oversampled to the 0.1 cm^{-1} grid. The residual was roughly minimized for a resolving power of 2000, as

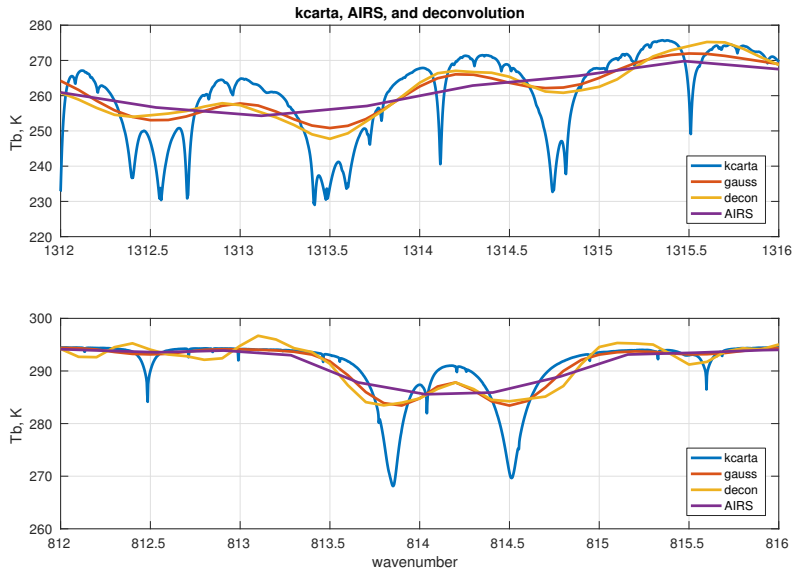

Figure 3: details from fitting profile 1 for kcarta, direct convolution to the 0.1 cm^{-1} grid ("gauss"), deconvolved AIRS, and true AIRS.

shown here. We also tried the generalized Gaussian with a fixed FWHM for values 0.4, 0.6, and 0.8, and a sinc basis with a spacing of 0.2 cm^{-1}, all of which gave larger residuals.

The AIRS deconvolution gives a modest resolution enhancement, at the cost of added artifacts and noise. Figure 3 shows details of kcarta, direct convolution to the 0.1 cm^{-1} grid ("gauss"), deconvolution, and AIRS spectra for fitting profile 1 [3, 5]. In the first subplot we see the deconvolution is capturing some of the fine structure in the kcarta data that is present in the direct convolution but not in the AIRS data. In the second subplot we see the deconvolution (and direct convolution) resolving a pair of close lines that are not resolved at the AIRS L1c resolution. But we also see some ringing that is not present in the direct convolution. Figure 4 shows the full spectra from fitting profile 1, along with sample details from the low and high ends of the band, for the deconvolution and direct convolution to the intermediate grid. In the details we see some overshoot and ringing in the deconvolution. But as noted we do not propose using the deconvolved radiances directly, they are an intermediate step in reconvolution to a lower resolution.

Figure 5 shows a pair of typical adjacent rows of the deconvolution matrix

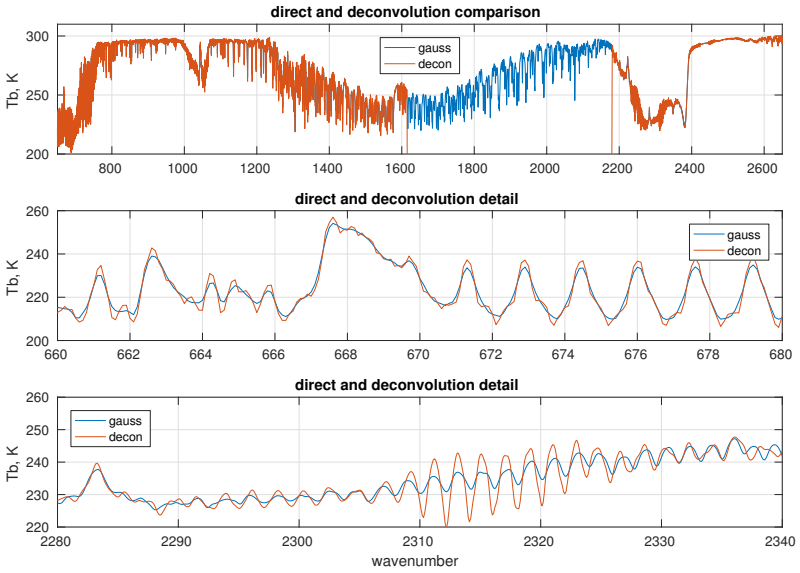

Figure 4: spectra from fitting profile 1 for direct convolution to the 0.1 cm^{-1} grid ("gauss") and deconvolved AIRS

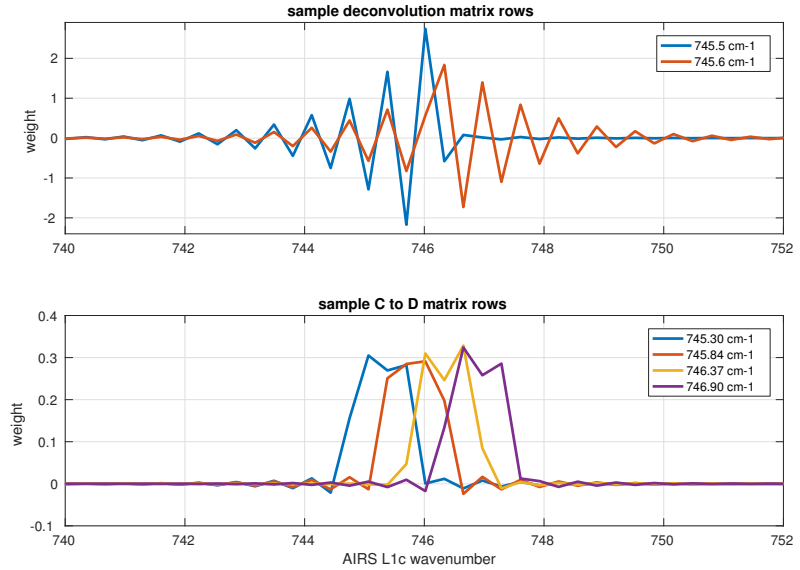

Figure 5: sample adjacent rows for the deconvolution and L1c to L1d transforms

S_b^{-1} in the first subplot. Row i of S_b^{-1} is the weights applied to L1c channel radiances to synthesize the deconvolved radiance r_i at the intermediate grid frequency v_i. The oscillation shows we are taking the closest AIRS channel, subtracting weighted values for channels ± 1 step away, adding weighted values for channels ± 2 steps away, and so on, with the weights decreasing quickly as we move away from v_i, with eight to ten L1c channels making a significant contribution to each deconvolution grid point.

The second subplot shows four adjacent rows of the matrix $S_d \cdot S_b^{-1}$, which takes L1c to L1d channel radiances. (The L1d radiances are discussed in a later section; here they are of interest mainly as a typical reconvolution.) Both matrices are banded but the bands are narrower in the second, with three to five L1c channels contributing significantly to each L1d channel. The range of influence is significant since for example we may want to see which L1d channels are derived in part from the subset of synthetic L1c channels.

3 AIRS to CrIS translation

Given AIRS deconvolution to a 0.1 cm^{-1} intermediate grid, reconvolution to the CrIS user grid is straightforward. For the CrIS standard resolution mode the channel spacing is 0.625 cm^{-1} for the LW, 1.25 cm^{-1} for the MW, and 2.5 cm^{-1} for the SW bands. For each CrIS band, we (1) find the AIRS and CrIS band intersection, (2) apply a bandpass filter to the deconvolved AIRS radiances restricting them to the intersection, with a rolloff outside the intersection, and (3) reconvolve the filtered spectra to the CrIS user grid with a zero-filled double Fourier transform [**?**].

Translations are tested by comparison with calculated reference truth. We start with a set of atmospheric profiles and calculate upwelling radiance at a 0.0025 cm^{-1} grid with kcarta [4] over a band spanning the domains of the AIRS and CrIS response functions. "True AIRS" is calculated by convolving the kcarta radiances with AIRS SRFs and "true CrIS" by convolving kcarta radiances to a sinc basis at the CrIS user-grid. True AIRS is then translated to CrIS to get "AIRS CrIS", and this is compared with true CrIS. Figure 6 shows sample spectra for true AIRS, deconvolved AIRS, true CrIS and AIRS CrIS. The difference between true CrIS and AIRS CrIS is hard to see at this level of detail, and for the remainder of this paper we will mainly show explicit differences.

For most tests we use a set of 49 fitting profiles spanning a wide range of clear atmospheric conditions, initially chosen for testing radiative transfer

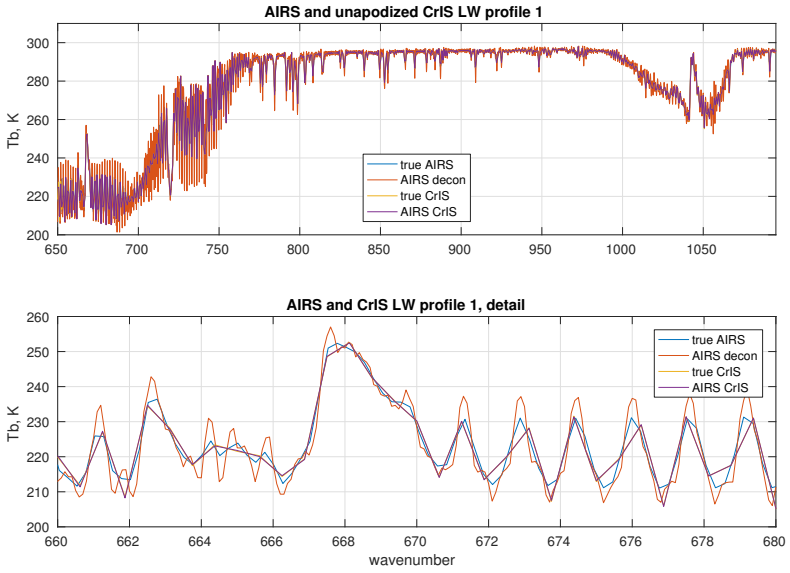

Figure 6: true AIRS, deconvolved AIRS, true CrIS, and AIRS CrIS

codes [3, 5]. The set is largely uncorrelated; reducing the reconstruction residual to 0.02 K requires 48 left-singular vectors. (Details of this correlation measure are given in an appendix.) For statistical correction and the direct regression discussed in section 5 we also use a set of 7377 radiances calculated from mostly cloudy AIRS profiles spanning several consecutive days as the dependent set. This set is moderately correlated; reducing the reconstruction residual to 0.02 K requires 260 left-singular vectors. Splitting the 7377 profile set into dependent and independent subsets and comparing residuals from the independent subset with residuals from the 49-profile set, we found residuals from the latter are consistently larger, suggesting it makes for a stricter test. So for the results shown here the test or independent set is always the 49-profile set, while for tests requiring fitting the 7377 profile is used as the dependent set.

Figures 7, 8, and 9 show the mean and standard deviation of true CrIS minus AIRS CrIS for the 49 fitting profiles, with and without Hamming apodization, for each of the CrIS bands. Figure 10 summarizes these results for Hamming apodized radiances. The residual has a high frequency component with a period of 2 channel steps that is significantly reduced by the apodization. The constant or DC bias is very close to zero for the apodized residuals.

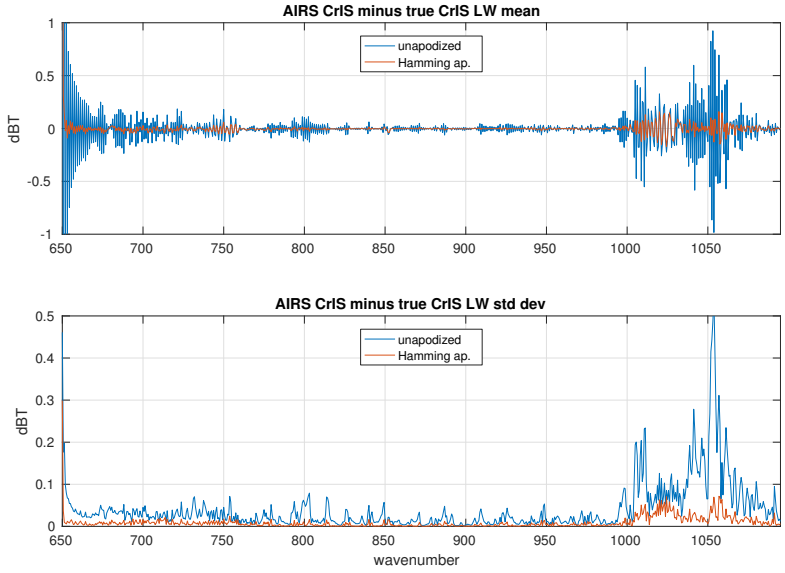

Figure 7: Mean and standard deviation of unapodized and Hamming apodized AIRS CrIS minus true CrIS, for the CrIS LW band

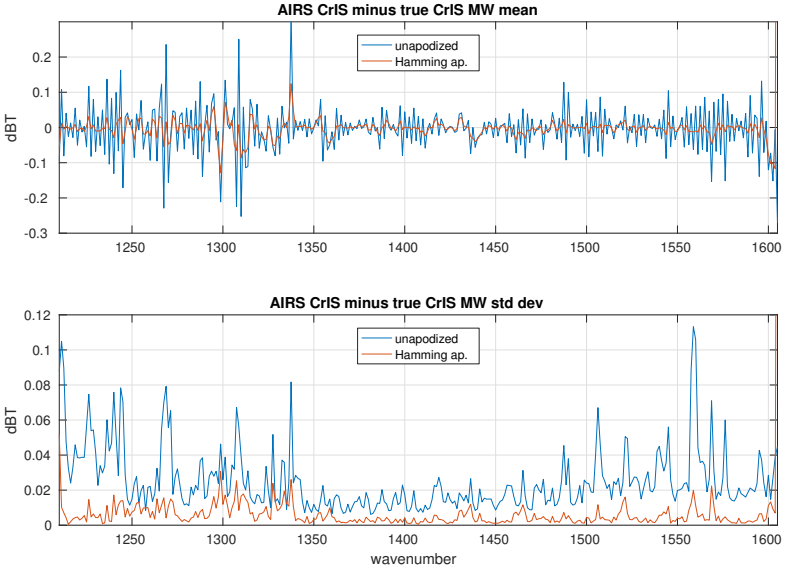

Figure 8: Mean and standard deviation of unapodized and Hamming apodized AIRS CrIS minus true CrIS, for the CrIS MW band

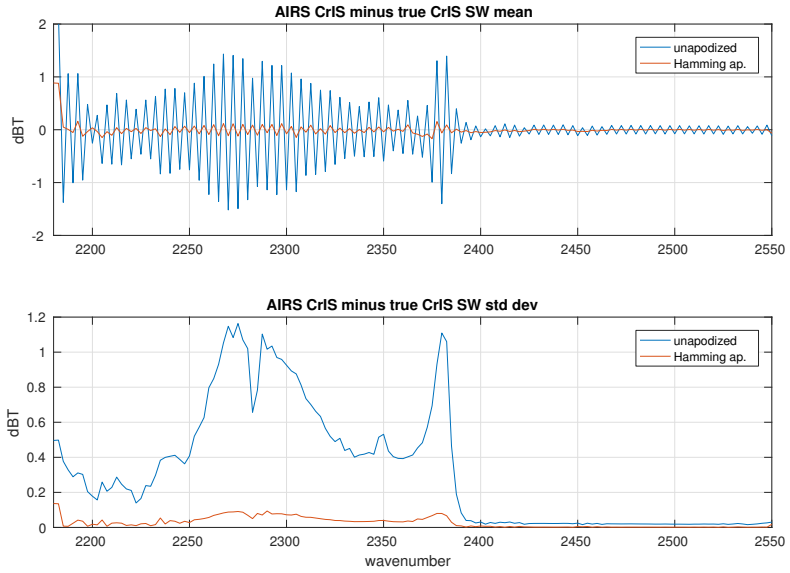

Figure 9: Mean and standard deviation of unapodized and Hamming apodized AIRS CrIS minus true CrIS, for the CrIS SW band

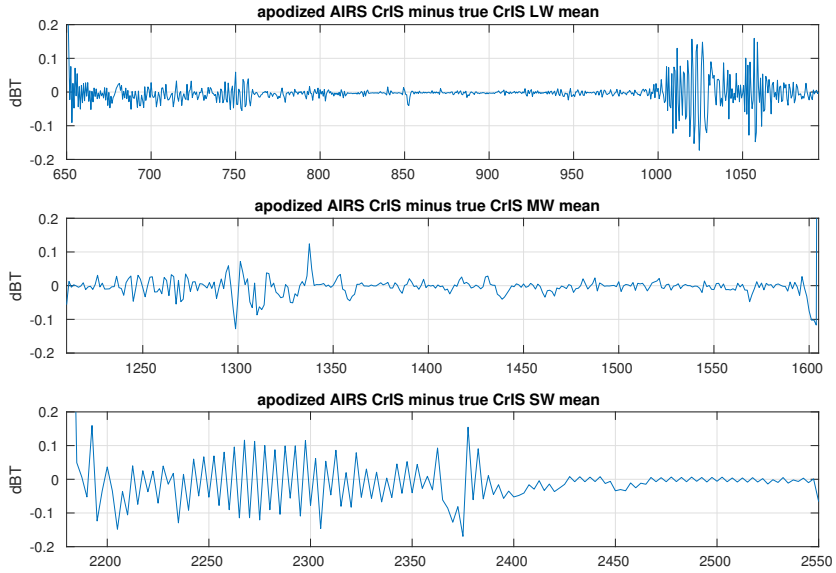

Figure 10: Mean of apodized residuals for all three CrIS bands

Some regularity remains in the apodized residual, including the oscillation with a period of two channel steps. Up to this point there as been no statistical component to our translation, beyond the choice of test set for validation. We feel it is important to be clear about any steps that require statistical fitting. That said, a simple linear correction can give a significantly further reduction of the residuals. For such tests as noted we use the set of 7377 mostly cloudy AIRS profiles as the dependent set and the 49 profile set the independent or test set.

We compare three such corrections. These are done with a separate regression for each CrIS channel, and so introduce no cross-correlations. Let t_i^{TC} be true CrIS and t_i^{AC} AIRS to CrIS brightness temperatures for CrIS channel i, from the dependent set. For the bias test we subtract the mean residual from the dependent set. For the linear test we find a_i and b_i to minimize $||a_i\, t_i^{\text{AC}} + b_i - t_i^{\text{TC}}||_2$, and for the quadratic test weights c_i, a_i and b_i to minimize $||c_i\, (t_i^{\text{AC}})^2 + a_i\, t_i^{\text{AC}} + b_i - t_i^{\text{TC}}||_2$. The resulting correction is then applied to the independent set, the 49 fitting profiles, for comparison with true CrIS.

Figure 11 is a comparison of bias, linear, and quadratic corrections for the LW band. The linear and quadratic corrections are nearly identical, and the quadratic coefficient is very close to zero. Figure 12 shows the weights for the linear fits from figure 11. The a weights are very close to 1 and the b weight to the bias. Figures 13 and 14 show the linear correction giving a similar improvement in the MW and a small improvement in the SW, where the quadratic correction is noticably worse. Figure 15 summarizes results for the linear correction, paired with the apodized uncorrected residuals.

We can give a reasonable estimate of noise equivalent differential radiance (NEdN) for the translation as follows. We start with AIRS L1c and CrIS NEdN estimates. These noise specs are showin in figure 16. The L1c spec is the average over a day (4 Dec 2016) of NEdN values from the L1c granules, with gaps for the synthetic channels filled by interpolation. The CrIS values are from a single CCAST **??** granule for the same day. The CCAST values are quite stable over time and consistent with NOAA CrIS NEdN estimates [**?**]. Noise with a normal distribution at the AIRS spec is added to true AIRS and then measured. The measured AIRS noise is the "test" line in the plot. This is very close to the spec and so serves as a check for our methods. True AIRS with added noise is then translated to CrIS and the noise of the translation is measured. This is the AIRS to CrIS line in the plots. The unapodized translation tracks the AIRS noise spec fairly closely in the LW and MW, and is a little less in the SW. Unapodized AIRS to CrIS noise is a little higher than true CrIS noise in the LW, a little less in the MW, and significantly less in the SW, and this relationship is unchanged with apodization.

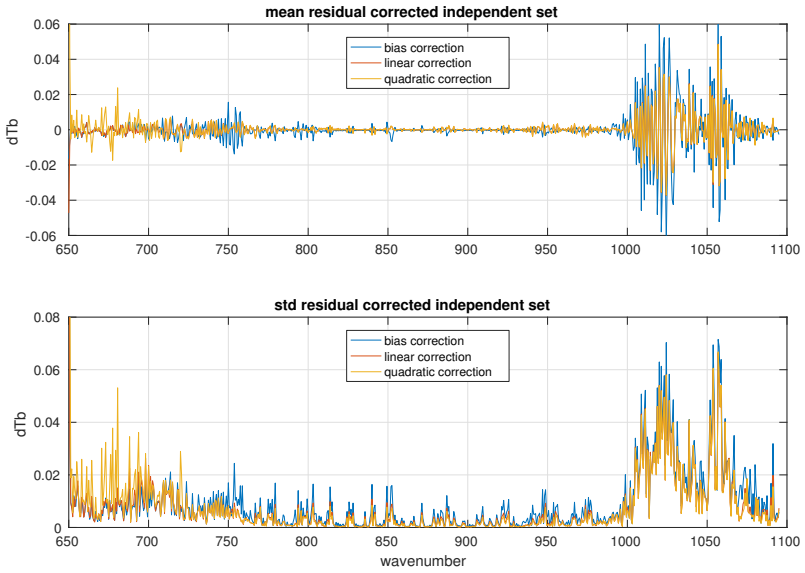

Figure 11: Mean and standard deviation of LW corrected apodized residuals

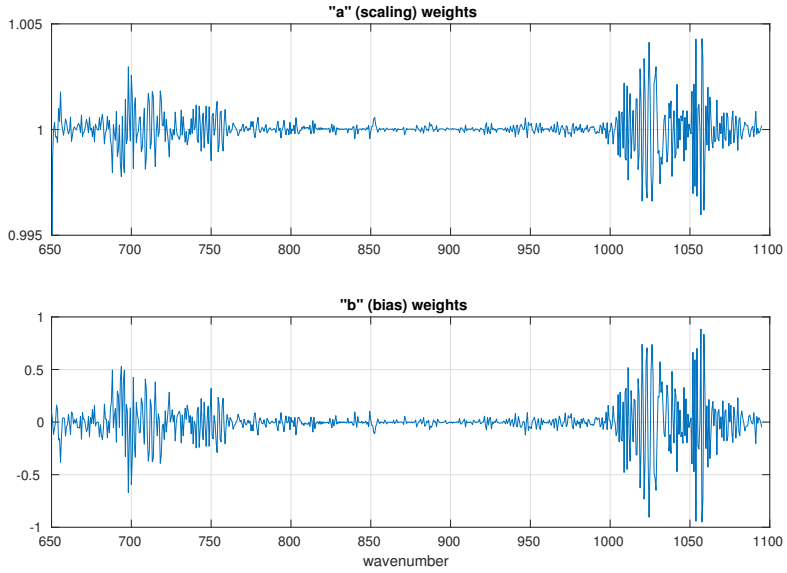

Figure 12: LW a and b weights for the linear correction $ax + b$

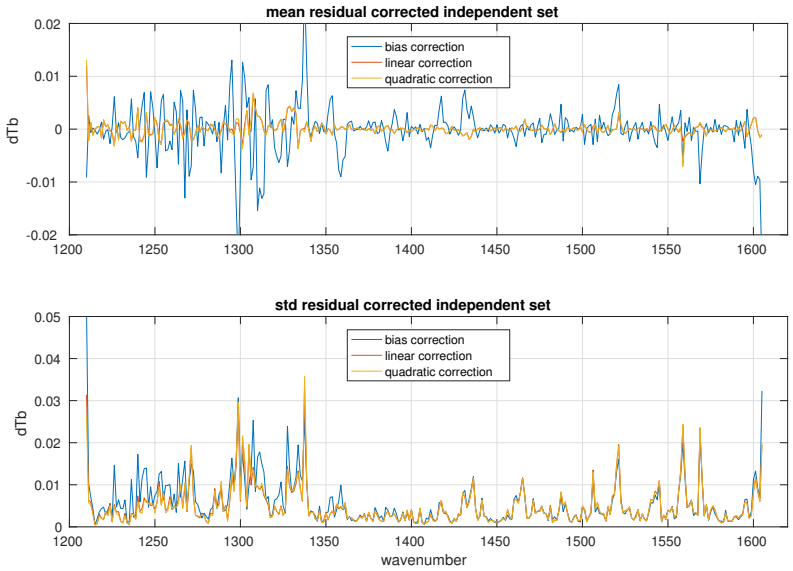

Figure 13: Mean and standard deviation of MW corrected apodized residuals.

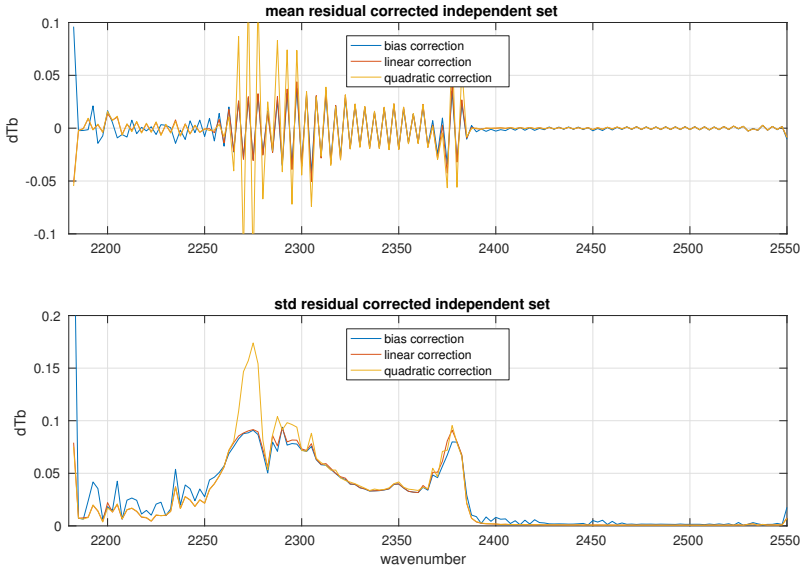

Figure 14: Mean and standard deviation of SW corrected apodized residuals.

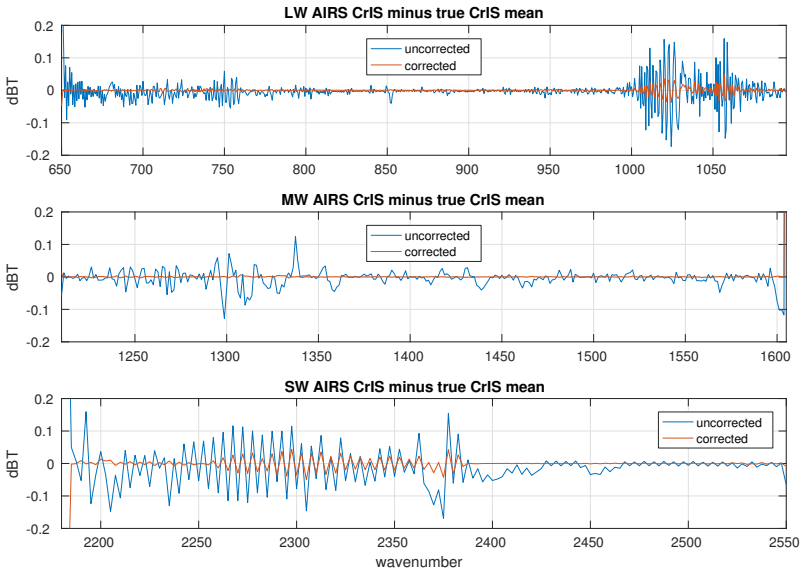

Figure 15: Mean corrected and uncorrected apodized residuals for all three bands.

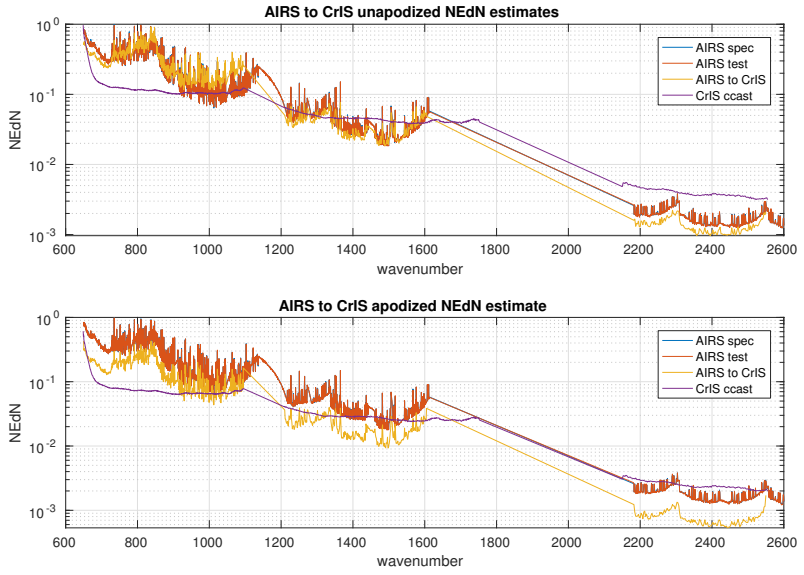

Figure 16: AIRS to CrIS unapodized and apodized NEdN estimates

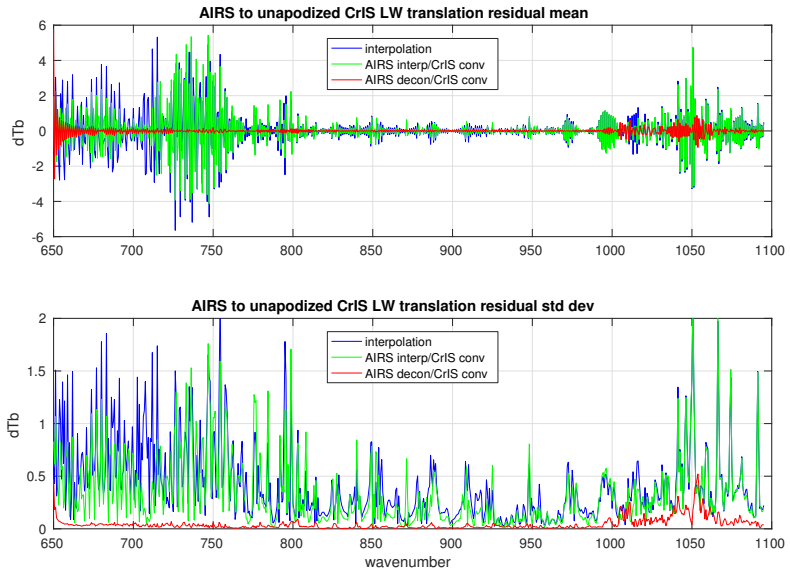

Figure 17: spline interpolation, interpolation with convolution, and deconvolution with convolution for the CrIS LW band

AIRS to CrIS translation via de- and re-convolution works significantly better than conventional interpolation. We consider two cases. For the first, start with true AIRS and interpolate radiances directly to the CrIS user grid with a cubic spline. For the second, interpolate true AIRS to the 0.1 cm^{-1} intermediate grid with a cubic spline and then convolve this to the use CrIS user grid. Figure 17 shows interpolated CrIS minus true CrIS for the LW band, without apodization. The two-step interpolation works a little better than the simple spline, but both residuals are significantly larger than for the translation with deconvolution. Results for the MW are similar, while the unapodized comparison is less clear for the SW. With Hamming apodization, the residuals with deconvolution are significantly less than interpolation for all three bands.

4 Translation to an idealized grating model

The AIRS deconvolution can be used for other translations. In this section we briefly consider reconvolution to an idealized grating model for resolving powers of 700 and 1200. Define an AIRS L1d basis with resolving power R from the generalized Gaussian response function of section 2 as follows.

Let v_0 be the frequency of the first channel and for $i \geq 0$ $\text{FWHM}_i = v_i/R$, $dv_i = \text{FWHM}_i/2$, and $v_{i+1} = v_i + dv_i$. As with tests of the AIRS to CrIS translation, true L1c is calculated by convolving kcarta radiances with AIRS L1c SRFs and true L1d by convolving with an L1d basis at the desired resolving power. L1c is translated to L1d by deconvolution followed by reconvolution to the desired L1d basis, and this is compared with true L1d.

Figure 18 shows residuals for reconvolution to an L1d basis with resolving power of 1200, the nominal AIRS resolution, and figure 19 shows residuals for a resolving power of 700. Note the different x-axes for the two figures. The residuals depend in part on the L1d starting channel v_0, and so on how the L1c and L1d SRF peaks line up. The residuals shown are the result of a rough fit for v_0. For a resolving power of 1200 this gave v_0 equal to the first L1c channel, while for 700 it was the first L1c channel plus 0.2 cm^{-1}.

We see that for both the AIRS to CrIS and L1c to L1d translations some resolving power is sacrificed in shifting channel centers to a single regular function of frequency. Residuals for a resolving power of 1200 (figure 18) are roughly comparable to unapodized CrIS (figures 7, 8, and 9) and residuals for a resolving power of 700 (figure 19) are roughly comparable to apodized CrIS (figure 15). As with the AIRS to CrIS translation, the L1c to L1d residuals are significantly reduced with a linear correction. Residuals for L1d with a resolving power of 700 after correction are comparable to residuals for apodized CrIS after a similar correction.

As with the AIRS to CrIS translation, deconvolution works significantly better than interpolation. We consider similar cases. For the first, start with true L1c and interpolate radiances directly to the L1d grid with a cubic spline. For the second, interpolate true L1c to the 0.1 cm^{-1} intermediate grid with a cubic spline and convolve this to the L1d channel set. Figure 20 shows interpolated L1d minus true L1d. The two-step interpolation works a little better than the simple spline, but is still much larger than the residual for translation with deconvolution.

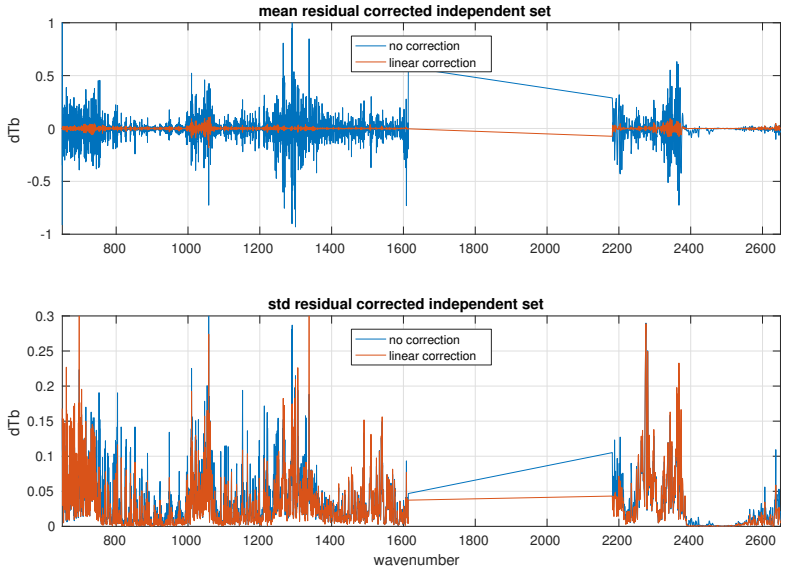

Figure 18: mean and standard deviation over the 49 fitting profiles for the L1c to L1d translation minus true L1d for a resolving power of 1200

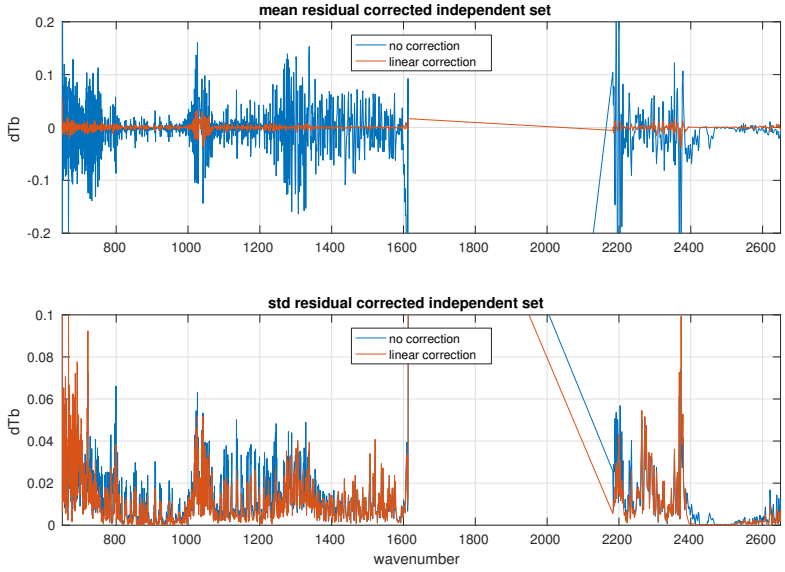

Figure 19: mean and standard deviation over the 49 fitting profiles for the L1c to L1d translation minus true L1d for a resolving power of 700

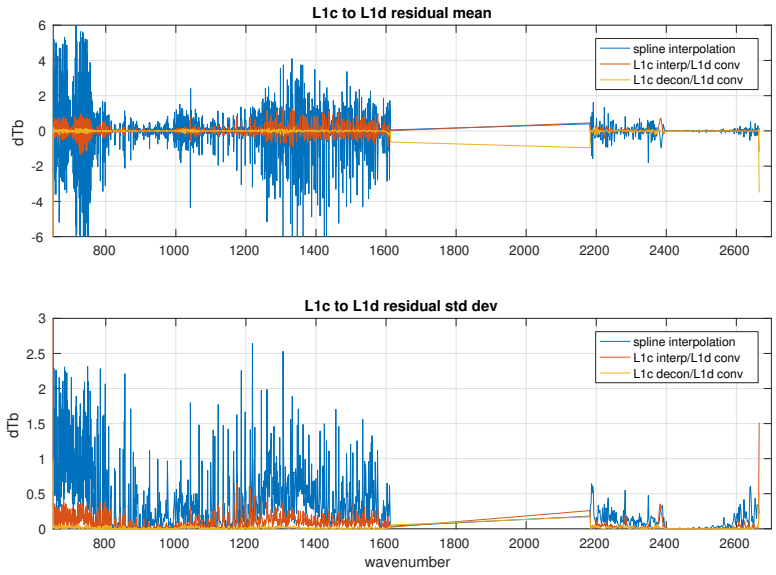

Figure 20: spline interpolation, interpolation with convolution, and deconvolution with convolution for the AIRS L1c to L1d translation with $v_0 = 649.822$ cm^{-1} and a resolving power of 700

5 Direct and principal component regression

The AIRS L1c to L1d translation can be done with a single linear transform $S_d \cdot S_c^{-1}$, where S_c and S_d are the transforms taking the intermediate grid to L1c and L1d channels. A similar one-step transform is possible for the AIRS to CrIS translation if we use a resampling matrix rather than double Fourier interpolation. We can get such a tranform in other ways. For example if r_a and r_c are $m \times k$ and $n \times k$ AIRS and CrIS radiance sets, we can find X to minimize $\|Xr_a - r_c\|_2$. Typically $k > m$, giving an overdetermined system, and we solve $r_a^t X^t = r_c^t$ for X by regression. This is different from the corrections of section 3 and 4; there regression was used to find linear or quadratic correction coefficients independently for each channel.

Figures 21 and 22 show residuals for direct regression and the deconvolution translation with statistical correction, both for apodized radiances. As with the translation corrections we use the 7377 profile set as the dependent and the 49 profile as the independent sets. The residuals are roughly comparable; the LW residual is larger at the low end of the band for direct regression and the high end for the deconvolved translation. Deconvolution does better in the MW, and direct regression in the SW.

The regression matrices show significant unwanted correlations. Figure 23 shows this for the LW; the MW and SW bands are much worse. As noted in section 3 the 7377 profile dependent set is highly correlated. The effective dimension is only 260, our regression is actually under-determined, and the dependent set residuals are very small. The independent set residuals are larger but acceptable because the 7377 profile set approximately spans the 49 profile test set.

One fix is to add noise. Recall that we generate true AIRS and true CrIS by convolving a common set of high-resolution radiances. For true AIRS we can simply add noise at the AIRS NEdN spec. But if we want true CrIS radiances with noise for testing or regression it does not work well to simply add noise at the CrIS NEdN spec. This does reduce correlations but increases residuals for the independent set significantly. To model NEdN for the AIRS to CrIS translation we synthesize noise at the AIRS NEdN spec, add it to the signal, run it through the translation, and measure it. Similarly, for testing or regression it might be better to generate true AIRS, generate noise at the AIRS NEdN spec, add this to true AIRS, translate the individual noise spectra to CrIS, and add these to true CrIS. The problem is getting a reference translation for the noise, and we do not pursue that further here.

As an alternative to adding noise, we can use a form of principal component regression. As above, r_a and r_c are $m \times k$ and $n \times k$ AIRS and CrIS radiance sets. Let $r_a = U_a S_a V_a^T$ be a singular value decomposition with singular values in descending order and U_a^i the first i columns of U_a. Similarly let $r_c = U_c S_c V_c^T$ be a singular value decomposition with singular values in descending order and U_c^j the first j columns of U_c. Let $\hat{r}_a = (U_a^i)^T r_a$ and $\hat{r}_c = (U_c^j)^T r_c$. This gives r_a and r_c represented with respect to the bases U_a^i and U_c^j. Since these are orthonormal, the transpose is the inverse. Then as before find X to minimize $\|X\hat{r}_a - \hat{r}_c\|_2$ by solving $\hat{r}_a^T X^T = \hat{r}_c^T$ for X by regression. Translating X a transform on the bases for r_a and r_c gives us $R = U_c^j X (U_a^i)^T$, our AIRS to CrIS transform. This is parameterized by i and j, the AIRS and CrIS basis sizes.

Figure 24 shows residuals and figures 25, 26, and 27 the final linear transform R for the CrIS LW, MW, and SW bands. We have chosen $i = j = 500$ for the LW, $i = 500$ and $j = 320$ for the MW, and $i = j = 100$ for the SW, to roughly balance unwanted correlation with residual size.

Note that this sort of principal component regression is not the same as regression after principal component (or singular vector) filtering; for that we would take $\bar{r}_a = U_a^i (U_a^i)^T r_a$, $\bar{r}_c = U_c^j (U_c^j)^T r_c$, find X to minimize $\|X\bar{r}_a - \bar{r}_c\|_2$, and have no need for a change of bases to apply X. In practice

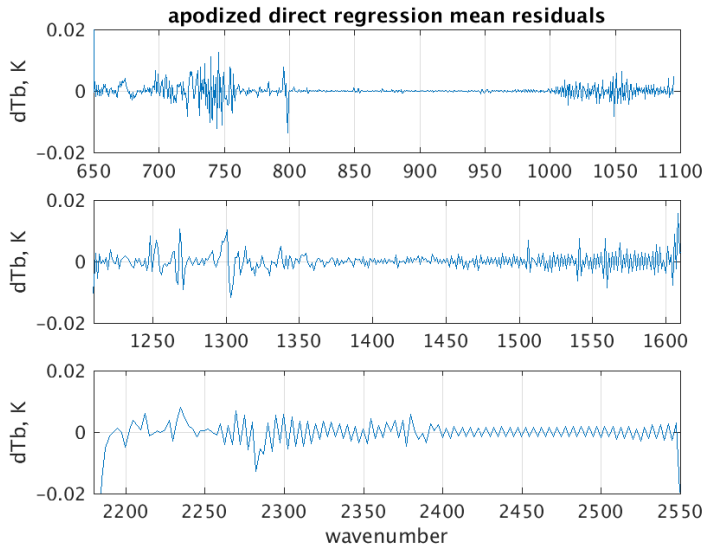

Figure 21: mean residuals for apodized AIRS to CrIS direct regression

this did not work as well as doing regression after the change of bases.

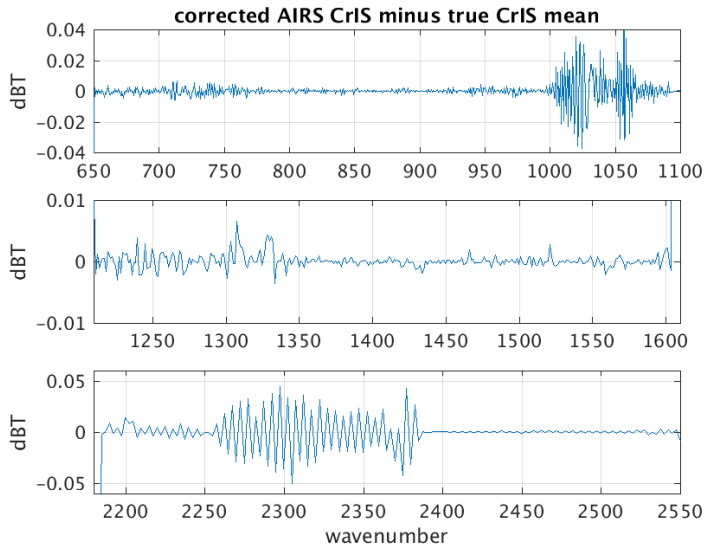

Figure 22: mean residuals for apodized AIRS to CrIS reconvolution with the regression correction

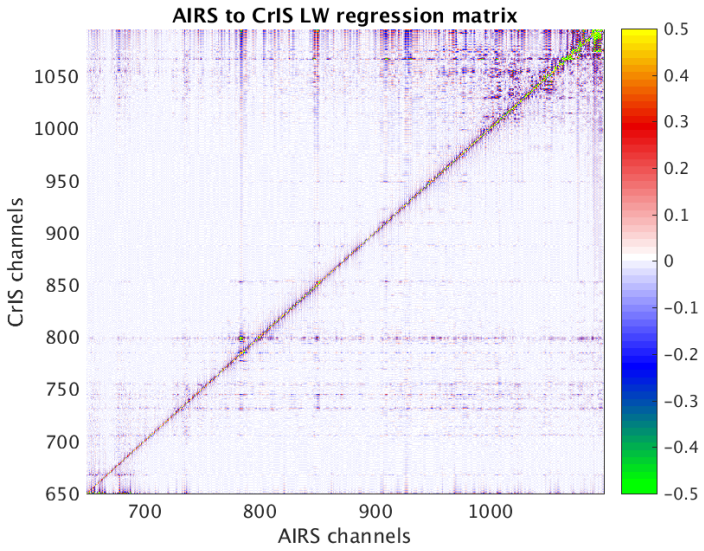

Figure 23: regression coefficients for the LW direct regression

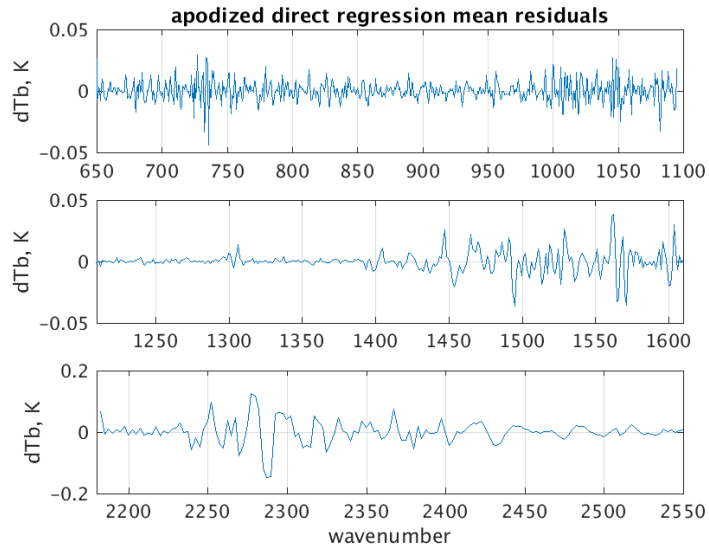

Figure 24: mean residuals for apodized AIRS to CrIS principal component regression

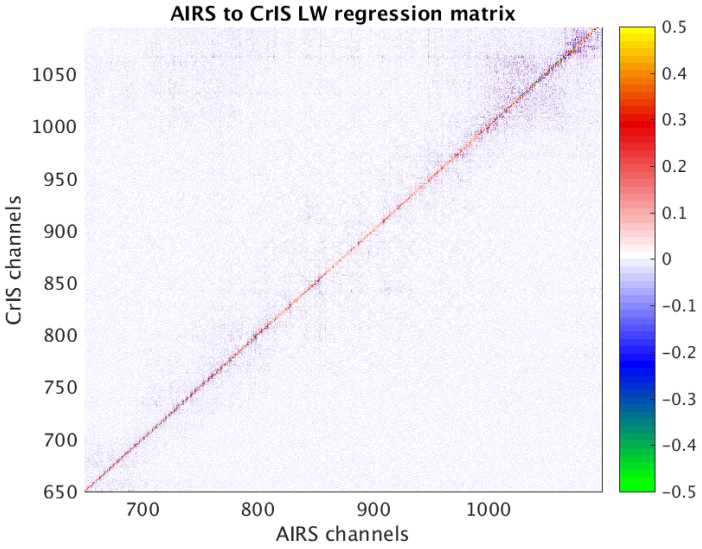

Figure 25: regression coefficients for the LW principal component regression

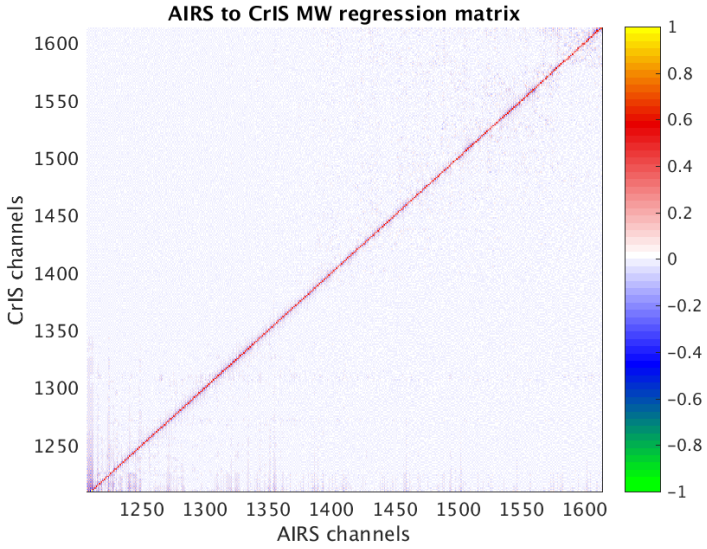

Figure 26: regression coefficients for the MW principal component regression

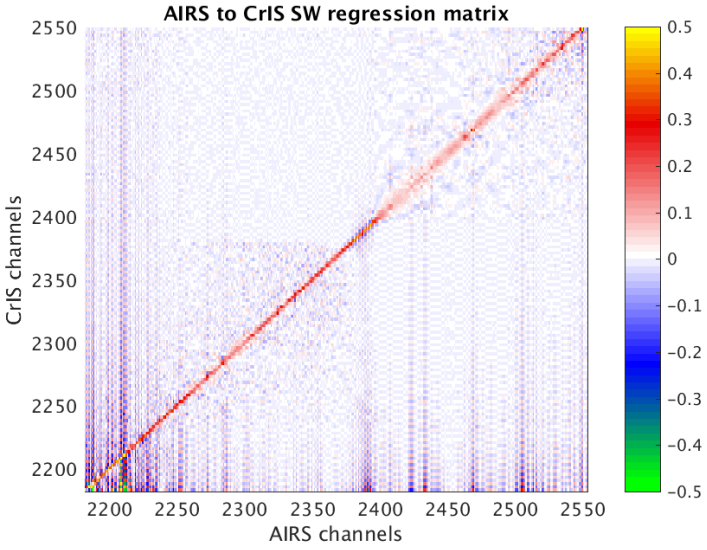

Figure 27: regression coefficients for the SW principal component regression

6 Conclusions

[rehash intro; maybe add some notes on applications and SNOs]

7 Appendix

We want to measure the correlation of a set of observations. A standard measure is the dimension of a spanning set. An analog when approximations are acceptable is to use the basis size needed to get a reconstruction residual below a fixed threshold. Let r_0 be an $m \times n$ array of radiances, one row per channel and one column per observation. Let $r_1 = USV^T$ be a singular value decomposition with singular values in descending order, and U_k the first k columns of U. Let $r_k = U_k U_k^T r_0$; then $r_k \approx r_0$. The approximation improves as k increases and becomes exact for some $k <= m$. This is the analog of principal component filtering using left-singular rather than eigenvectors. This is useful as a form of compression when k is small relative to n. For that case we save U_k and $U_k^T r_0$ separately. Applications include IASI radiance data and the kcarta absorption database.

Let B^{-1} be the inverse Planck function and define $d(r_1, r_2) = \text{RMS}(B^{-1}(r_1, v) - B^{-1}(r_2, v))$, the RMS difference over all channels and observations of the brightness temperatures of radiance data. Finally let j be the smallest value such that $d(r_0, r_j) \leq T_d$, for some threshold T_d. We have chosen as $T_d = 0.02$ K. Then j is the effective dimension of our set r_0. For the 49 profile fitting set this gives $j = 48$, which we would interpret as largely uncorrelated, while for the 7377 profile cloudy set we found $j = 260$, which we would interpret as highly correlated.

References

[1] H. H. Aumann, M. T. Chahine, C. Gautier, M. D. Goldberg, E. Kalnay, L. M. McMillin, H. Revercomb, P. W. Rosenkranz, W. L. Smith, D. H. Staelin, L. L. Strow, and J. Susskind. AIRS/AMSU/HSB on the aqua mission: design, science objectives, data products, and processing systems. *IEEE Transactions on Geoscience and Remote Sensing*, 41:253–264, Feb. 2003.

[2] Y. Han, H. Revercomb, M. Cromp, D. Gu, D. Johnson, D. Mooney, D. Scott, L. Strow, G. Bingham, L. Borg, Y. Chen, D. DeSlover, M. Esplin, D. Hagan, X. Jin, R. Knuteson, H. Motteler, J. Predina, L. Suwinski, J. Taylor, D. Tobin, D. Tremblay, C. Wang, L. Wang, L. Wang,

and V. Zavyalov. Suomi NPP CrIS measurements, sensor data record algorithm, calibration and validation activities, and record data quality. *Journal of Geophysical Research (Atmospheres)*, 118:12734, Nov. 2013.

[3] L. Strow, S. Hannon, S. De Souza-Machado, H. Motteler, and D. Tobin. An overview of the airs radiative transfer model. *Geoscience and Remote Sensing, IEEE Transactions on*, 41(2):303–313, Feb 2003.

[4] L. Strow, H. E. Motteler, R. G. Benson, S. E. Hannon, and S. D. Souza-Machado. Fast computation of monochromatic infrared atmospheric transmittances using compressed look-up tables. *Journal of Quantitative Spectroscopy and Radiative Transfer*, 59(35):481 – 493, 1998. Atmospheric Spectroscopy Applications 96.

[5] L. L. Strow, S. E. Hannon, S. De-Souza Machado, H. E. Motteler, and D. C. Tobin. Validation of the atmospheric infrared sounder radiative transfer algorithm. *Journal of Geophysical Research: Atmospheres*, 111(D9), 2006. D09S06.

[6] L. L. Strow, H. Motteler, D. Tobin, H. Revercomb, S. Hannon, H. Buijs, J. Predina, L. Suwinski, and R. Glumb. Spectral calibration and validation of the Cross-track Infrared Sounder on the Suomi NPP satellite. *Journal of Geophysical Research (Atmospheres)*, 118:12486, Nov. 2013.